AIP | Journal of Applied Physics

Temperature dependent dynamics transition of intermittent plastic flow in a metallic glass. I. Experimental investigations

Z. Y. Liu, G. Wang, K. C. Chan, J. L. Ren, Y. J. Huang et al.

Citation: J. Appl. Phys. **114**, 033520 (2013); doi: 10.1063/1.4815943
View online: http://dx.doi.org/10.1063/1.4815943
View Table of Contents: http://jap.aip.org/resource/1/JAPIAU/v114/i3
Published by the AIP Publishing LLC.

Temperature dependent dynamics transition of intermittent plastic flow in a metallic glass. I. Experimental investigations

Z. Y. Liu,[1,2] G. Wang,[1,a)] K. C. Chan,[2,a)] J. L. Ren,[3] Y. J. Huang,[4] X. L. Bian,[1] X. H. Xu,[5] D. S. Zhang,[6] Y. L. Gao,[1] and Q. J. Zhai[1]
[1]*Laboratory for Microstructures, Shanghai University, Shanghai 200444, China*
[2]*Department of Industrial and System Engineering, The Hongkong Polytechnic University, Hongkong, China*
[3]*Department of Mathematics, Zhengzhou University, Zhengzhou 450001, China*
[4]*School of Materials Sciences and Engineering, Harbin Institute of Technology, Harbin 150001, China*
[5]*Institute of Mechanics, Chinese Academy of Sciences, Beijing 100083, China*
[6]*Department of Mechanics, Shanghai University, Shanghai 200444, China*

(Received 16 March 2013; accepted 2 July 2013; published online 18 July 2013)

Cooling shrinkage can increase the atomic packing density of metallic glasses, which can influence their elastic and plastic behaviour. In the present study, the compressive deformation behaviour of a Zr-based metallic glass at temperatures well below the glassy transition temperature, say 123 K to room temperature, is experimentally revealed. The elastic modulus and the shear modulus at different temperatures are measured to elucidate the yield strength changes with temperature according to the model of shear transformation zones. In the plastic regime, based on the SEM observation and the digital scattering correlation method, an enhanced interaction between the elastic shear strain fields initiated by neighbouring shear bands is discussed, which explains the amplitude of serration events decreasing with the temperature decreasing. © *2013 AIP Publishing LLC*. [http://dx.doi.org/10.1063/1.4815943]

I. INTRODUCTION

In metallic glasses, plastic deformation is manifested by serrated flow or repeated yielding, and the serration events are associated with the shear band formation and propagation.[1] After analysing the elastic energy aggregation and release in serration events, a phenomenological model was established to schematically examine the correlation between the shear banding and serration events of metallic glasses.[2] In order to quantitatively describe the deformation mechanism of metallic glasses, a number of theories such as the shear transformation zone (STZ) theory,[3] the free volume theory,[4] and the potential energy landscape (PEL) theory have been proposed.[5] The theories of STZ and free volumes construct a deformation unit to quantitatively describe the shear deformation in glassy materials.[6] The PEL theory maps all possible conformations of the deformation unit and reflects the corresponding energy levels of these conformations,[7] which forms a basis for quantitatively characterizing the thermally activated STZs in metallic glasses (viz., the size and activation energies), and the yielding behaviour.[8,9] Over the last few years, there have also been many research efforts to study the deformation mechanisms of metallic glasses with variant structures, such as nanocrystals or heterogeneities,[2,10] and under different testing temperatures.[11–14] It is well known that metallic glasses can achieve very large ductility when the testing temperature is higher than the glassy transition temperature, which makes metallic glasses undergo viscous flow in the supercooled liquid region and approach a superplasticity.[11,12] Recently, some studies have also demonstrated that low temperatures could reduce the mobility of atoms,[13,14] change the dynamic behaviour of the shear banding,[15–17] and then improve the yield strength and plastic deformation ability of metallic glasses.[13,18] However, these observations do not elucidate the plastic mechanism of metallic glasses at low temperature, particularly, the spatial interaction of the deformation medium, i.e., shear bands, has not been reported.

In the present study, the deformation behaviour of a metallic glass, $Zr_{41.25}Ti_{13.75}Ni_{10}Cu_{12.5}Be_{22.5}$ (at. %) at temperatures well below glassy transition temperature, i.e., 123 K to 300 K, is investigated. The stress-time curves at different low temperatures are studied to characterize the serrated flow behaviour. Spatial interactions between the shear bands are also elucidated by simulating the elastic strain fields at the tip of the shear bands in order to provide a better understanding of serrated flow behaviour in metallic glasses.

II. EXPERIMENTAL PROCEDURE

The $Zr_{41.25}Ti_{13.75}Ni_{10}Cu_{12.5}Be_{22.5}$ alloy was prepared by arc melting appropriate amounts of pure metal elements, with purities higher than 99.99%, in an argon atmosphere. The alloy was then injected into copper mould to form a rod-like metallic glass (2 mm diameter; 70 mm length) and a plate-like metallic glass sample ($3 \times 30 \times 70\,mm^3$). The glassy phase structures of each cast specimen were examined by X-ray diffraction (XRD), and the fractography of the specimens was observed with a JEOL JSM-6335F scanning electron microscope (SEM). The thermal properties of the metallic glass were measured using a Perkin-Elmer Pyris differential scanning calorimeter (DSC) at a heating rate of 20 K/min. Compression specimens with a length/diameter ratio of 2 were cut from the rod-like metallic glass sample, and the ends of each specimen were carefully ground to a surface

a)Authors to whom correspondence should be addressed. Electronic addresses: g.wang@shu.edu.cn and mfkcchan@inet.polyu.edu.hk.

roughness of 1 μm. Compression tests were conducted using an Instron 5500R machine equipped with an environmental box with a temperature accuracy of ± 2 K at a temperature range of 123–293 K and strain rate of 2.5×10^{-4} s^{-1}.

The elastic parameters were measured by a modulus and internal friction analyser (Nihon Techno-Plus Company, Japan). Elastic modulus measurement was conducted in a temperature range of 103–623 K in a JE-LT attachment and internal friction analyser by the free vibrational method (vibrational frequency of approximately 1000 Hz). The shear modulus between room temperature and 623 K was measured in a JG-RT attachment of the modulus and internal friction analyser at a similar vibrational frequency. Specimens subjected to elastic parameter measurements were sized $50 \times 10 \times 1$ mm^3.

To simulate the elastic strain fields at the tip of the shear band, a point load was applied to the surface of the metallic glass using an indenter constructed of a hard Cobalt-based alloy. The experimental setup is illustrated in Fig. 1(a). The geometric size of the Zr-based metallic glass is shown in Fig. 1(a). The indenter is a triangular prism with a length, L, of 20 mm and a height, H, of 10 mm. The angle of the indenter tip is 60°, and its radius is approximately 100 μm. An elastic strain field was activated beneath the loading point. The strain field was observed by the white digital speckle correlation method (DSCM). DSCM is a non-contact optical method for full-field displacement and strain measurements that require digital images captured before and after deformation.[19] In the present measurements, the surface of the sample was firstly spray-painted to generate artificial speckles and then illuminated by two fibre optic white light sources during loading. The painted surface of the sample under the indenter is shown in Fig. 1(b). A CCD video camera (JAI CV-A1) was placed in the front of the spray-painted surface to acquire the sequential speckle images necessary for performing digital speckle correlation (Fig. 1). The indentation moving speed was 1 μm/s, with a maximum load approaching 500 N. During the loading process, consecutive surface images were recorded with a 768×576 pixel CCD array and a length-pixel ratio of approximately 12.7 μm/pixel. The sequential images acquiring frequency was 2 Hz. A 100×100 pixel (1.27×1.27 mm) calculated domain was located beneath the loading point (Fig. 1). An image was obtained prior to loading that served as the reference (un-deformed) condition. The sequential images were analysed with respect to this reference condition using DSCM, that can provide a displacement resolution in 0.01 subpixels, i.e., approximately 0.1 μm by a combination of the sub-pixel technique and the Newton-Raphson iteration algorithm. The strain distribution at different loads could then be identified by a series of pronounced contour maps.[20]

III. RESULTS

The nominal stress-time curves of the $Zr_{41.25}Ti_{13.75}Ni_{10}Cu_{12.5}Be_{22.5}$ metallic glass, compressed at different temperatures, are plotted in Fig. 2(a). Because the extensometer could not be operated at low temperatures, plastic strain measurements are not provided in the present study. Thus, the deformation time is used to generate an estimate of the plastic strain. The resultant mechanical properties are outlined in Table I. These compression tests suggest that a decrease of the test temperature can increase the yield strength and the deformation time (corresponding to plasticity), and the effect is most notably at temperatures lower than 203 K.

By enlarging the plastic regime at room temperature, intermittent plastic flow is observed in the form of numerous serration events, as shown in Fig. 2(b). As the temperature decreases from 293 K to 203 K, the serration event amplitudes correspondingly decrease from ~25 MPa to ~4 MPa. When the temperature continues to decrease, accurate fluctuation of the stress due to the serration events cannot be discerned because of competing stress fluctuations generated by the vibrations of the machine and the friction between the cross-head of the Instron machine and the two ends of the compressed sample (Fig. 2(b)). In order to illustrate the influence of the vibration and friction from the Instron machine on the stress-time curves, the stress-time curve of the metallic glass deformed at 293 K, as shown in Fig. 3, is chosen as an example. Theoretically, the elastic deformation of metallic glasses must exhibit a perfect linear behaviour. However, by enlarging the stress-time curve in the elastic deformation stage (enclosed in the rectangle in Fig. 3(a)), small stress fluctuations (the inset of Fig. 3(a)) which are generated by the vibration and the friction can easily be seen. Through linear fitting in the elastic deformation stage, a baseline (or an ideal linear elastic stress-strain curve) is plotted in Fig. 3(a). When the experimental stress-time curve subtracts the baseline, the background noise amplitude of approximately 4 MPa can be calculated, as shown in Fig. 3(b). In order to eliminate the effect of the vibration and friction, serration events with a stress drop of less than 4 MPa in the plastic strain regime will be excluded in our analysis. Therefore, the stress fluctuations observed at temperatures below 203 K can be treated as background noise.

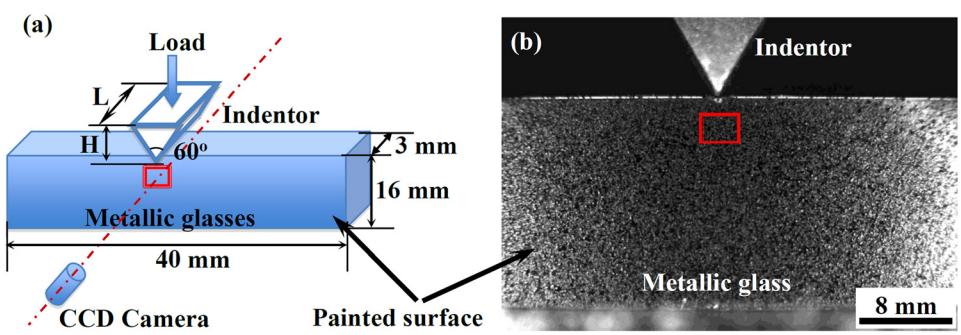

FIG. 1. The profile at point loading on the metallic glass. (a) Geometrical sketch of the indenter and the experimental setup. (b) The speckle image recorded by CCD camera. The rectangular area indicates the area used to calculate the elastic strain field by DSCM.

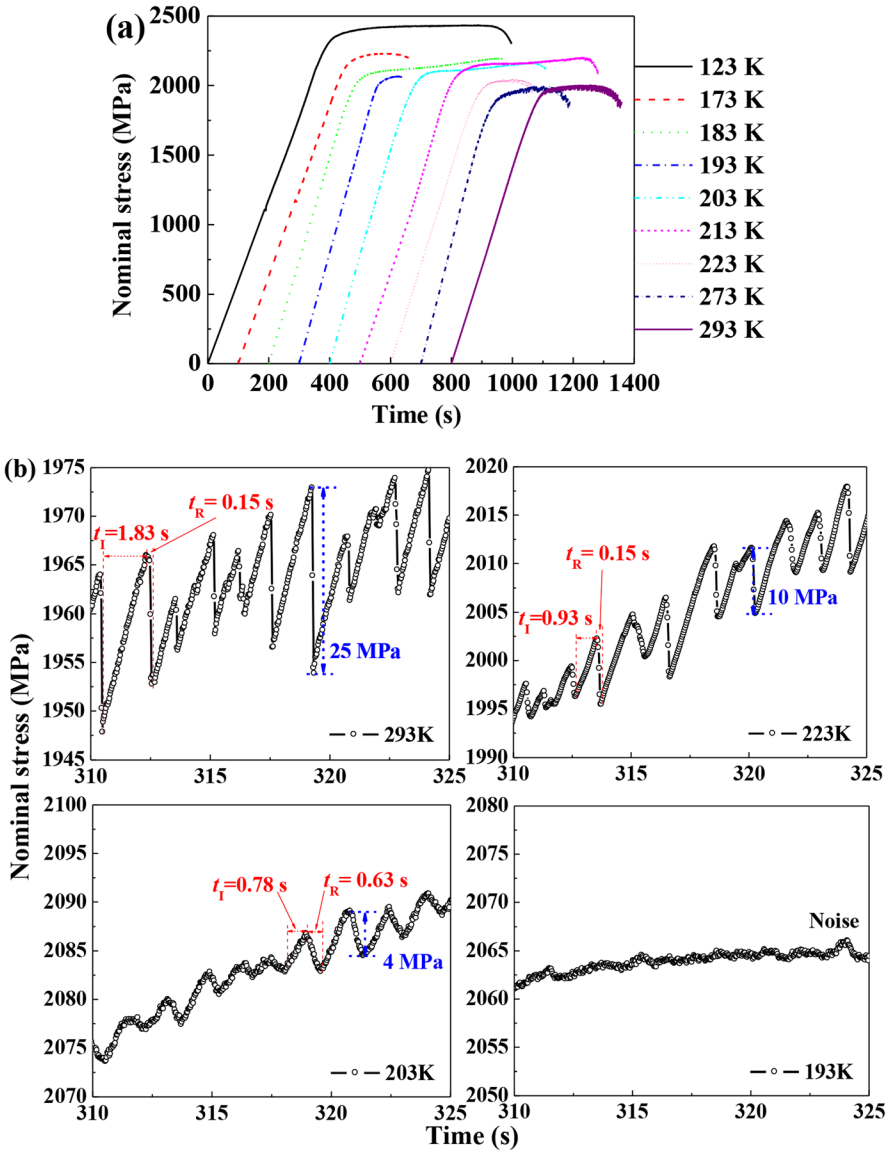

FIG. 2. Compression deformation of the $Zr_{41.25}Ti_{13.75}Ni_{10}Cu_{12.5}Be_{22.5}$ metallic glass at different temperatures. (a) Nominal stress-time curves at different temperatures. (b) Enlarged stress-time curves at the temperatures of 293 K, 273 K, 203 K, and 193 K.

The elastic parameters (elastic modulus and shear modulus) as functions of temperature are shown in Fig. 4. A DSC trace of the metallic glass is used to correlate these results with the structural evolution of the material, demonstrating that the glassy transition temperature (T_g) occurred at approximately 600 K. Before reaching T_g, an exothermic event is observed at a temperature range from approximately 480 K (the relaxation temperature, T_r) to 600 K. This reaction is generally believed to be the structural relaxation of the glassy phase.[21] The structural relaxation would induce the annihilation of the defects, such as the free volume.[21] The reduction in the free volume leads to the metallic glass being densified that results in the increment of the elastic modulus in the temperature ranged from 480 K to 600 K.[21] Thus, the experimentally measured elastic modulus in the temperature ranged from 480 K to 600 K exhibits an increase from 86.3 GPa to 89.6 GPa. The elastic modulus is observed to decrease from 91.8 GPa to 88.9 GPa between 103 and 293 K. Due to the limitation of the modulus and internal friction analyser, the shear moduli are only measured from 302 K to 462 K. The elastic modulus decreases by approximately 3.3% as the temperature increases from 103 K to 293 K.

TABLE I. Mechanical properties of the BMG compressed at different temperatures. T is temperature, τ_{CT} is critical shear stress, σ_Y is yield strength, σ_{FT} is fracture strength, γ_{CT} is critical shear strain, D_S is the average interval space between neighbouring shear bands, and θ_C is the fracture shear angle.

T (K)	σ_{FT} (MPa)	τ_{CT} (MPa)	γ_{CT}	σ_Y (MPa)	θ_C	D_S (μm)
293	1880 ± 48	927	0.0289	1660 ± 20	41°	~100
273	1890 ± 33	931	0.0289	1690 ± 16	41°	~100
223	1950 ± 55	966	0.0297	1730 ± 19	41°	~70
213	2080 ± 18	1035	0.0318	1850 ± 24	42°	~60
203	2120 ± 22	1053	0.0323	1900 ± 23	42°	~40
193	2060 ± 16	1023	0.0313	1930 ± 23	42°	~30
183	2180 ± 10	1089	0.0333	1920 ± 17	43°	~30
173	2190 ± 14	1090	0.0333	2070 ± 22	43°	~20
123	2400 ± 10	1180	0.0358	2260 ± 11	50°	~20

The lateral surfaces of specimens fractured at different temperatures are observed by SEM (Fig. 5). Numerous shear bands are visible on the surface of the fractured specimens, indicated by the arrows in Fig. 5. As the temperature decreases, the angle between the loading direction and the shear fracture surface (shear fracture angle) increases from

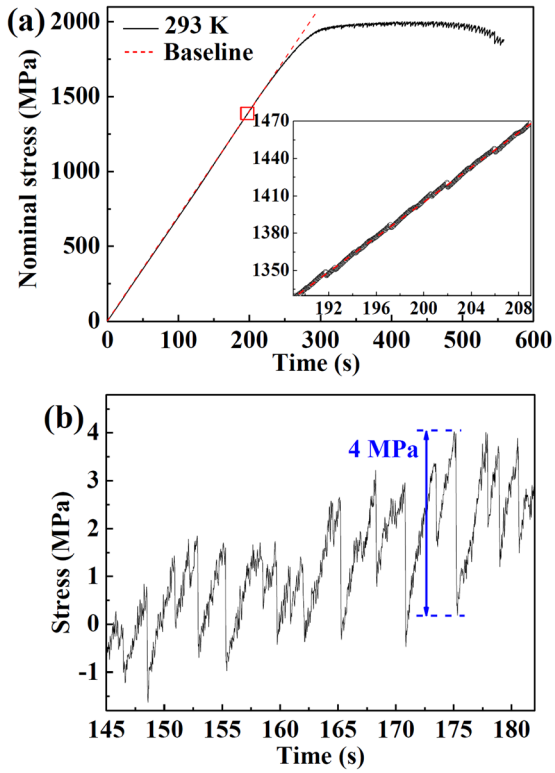

FIG. 3. Influence from the vibration and friction of the Instron machine. (a) Strain fluctuation in elastic deformation stage. (b) Calculation of the stress vibration amplitude.

41° at 293 K to 50° at 123 K, as shown in the insets of Fig. 5. These results confirm that the deformation is governed by shear fracture. The density of the shear bands also increases with decreasing temperature, marked by the arrows in Fig. 5, consistent with previous studies.[13,18] By measuring the interval space between neighbouring shear bands from the SEM images in five different regions, the averaged interval spaces are found to decrease from approximately 100 μm at room temperature to 20 μm at 123 K, as listed in Table I.

Additionally, numerous very weak shear bands with characteristic shortened lengths are also observed (Fig. 6), becoming increasingly obvious when decreasing the temperature from 293 K to 203 K (Fig. 6(a)). When the temperature approaches 183 K and 123 K, the densities of these short shear bands significantly increases (Figs. 6(b) and 6(c)), causing the spacing between the short shear bands to further decrease.

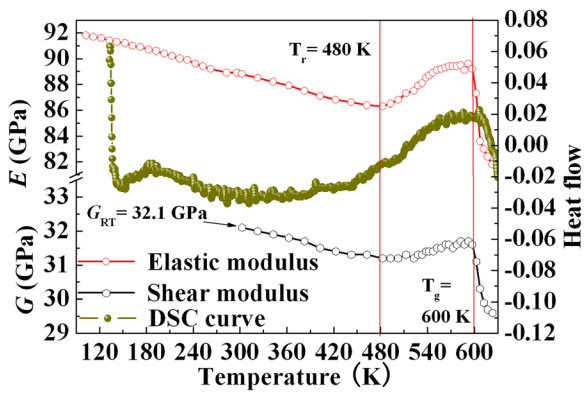

FIG. 4. Shear Modulus and Young's Modulus as functions of temperature measured by the elastic parameter and internal friction system. For comparison, the DSC trace of the $Zr_{41.25}Ti_{13.75}Ni_{10}Cu_{12.5}Be_{22.5}$ metallic glass is also plotted.

To find the elastic field distribution in the tip of the shear bands, indentation is used to stimulate the elastic strain field beneath the indenter (Fig. 1). Contour maps are generated for the linearly elastic strain (along the loading direction) field and the shear elastic strain field at a load of 10 N, as shown in Figs. 7(a) and 7(b), respectively, exhibiting obscurely linear elastic strain fields and shear elastic strain fields. At a load of 360 N, the strain concentration becomes more significant, revealing the presence of both linear elastic strain fields and shear elastic strain fields directly beneath the indenter, as shown in Figs. 7(c) and 7(d), respectively. On further increasing the load to 500 N, the range of the elastic strain field does not change significantly, while the maximum linear strain and shear strain increase (Figs. 7(e) and 7(f)). By analysis the cross sections of the shear strain fields along the dash lines in Figs. 7(b)–7(d), which indicates the direction perpendicular to the loading direction and the location very close to the loading point, the shear strains are plotted in Fig. 7(g), demonstrating that the maximum shear strain values at the three loads are approximately 0.002, 0.037, and 0.048, respectively. The maximum shear strain at a load of 500 N is consistent with the critical shear strain of 0.036 previously reported for the plastic yielding of metallic glasses.[22] Furthermore, the width of the shear elastic strain field is measured to be approximately 600 μm.

IV. DISCUSSION

It is evident that decreasing temperature brings out significant changes in the mechanical behaviour of the $Zr_{41.25}Ti_{13.75}Ni_{10}Cu_{12.5}Be_{22.5}$ metallic glass. The yield strength is obviously improved from 1660 MPa at room temperature to 2260 MPa at 123 K (cf. Fig. 2(a)). The plastic strain ability also is improved, which is consistent with previous studies.[14,18] The DSC trace suggests that the phase transformation does not change with decreasing temperature (cf. Fig. 4). Thus, the improvements in the yield strength and the plastic strain ability do not result from the glassy phase transformation. Due to the absence of crystallographic defects, the dislocation-mediated deformation mechanism in crystalline materials cannot be applied in metallic glasses. On the other hand, our SEM images clearly show that the plastic flow behaviour is still dominated by the shear banding mechanism, which does not change with decreasing temperature. Considering this evidence, we will elucidate the elastic deformation based on the elastic parameters analysis (cf. Fig. 4) and the plastic deformation based on the elastic field observations (cf. Fig. 7).

Elastic deformation is an elastic energy accumulation process. The elastic energy stored in the glassy phase must activate some structural evolutions.[23,24] However, direct investigation of the elastic structural evolution is difficult. As such, the elastic modulus change with temperature is used to characterize the relationship between the structure and yield behaviour of a metallic glass. Further enlarging the elastic modulus in the temperature range from 123 K to room

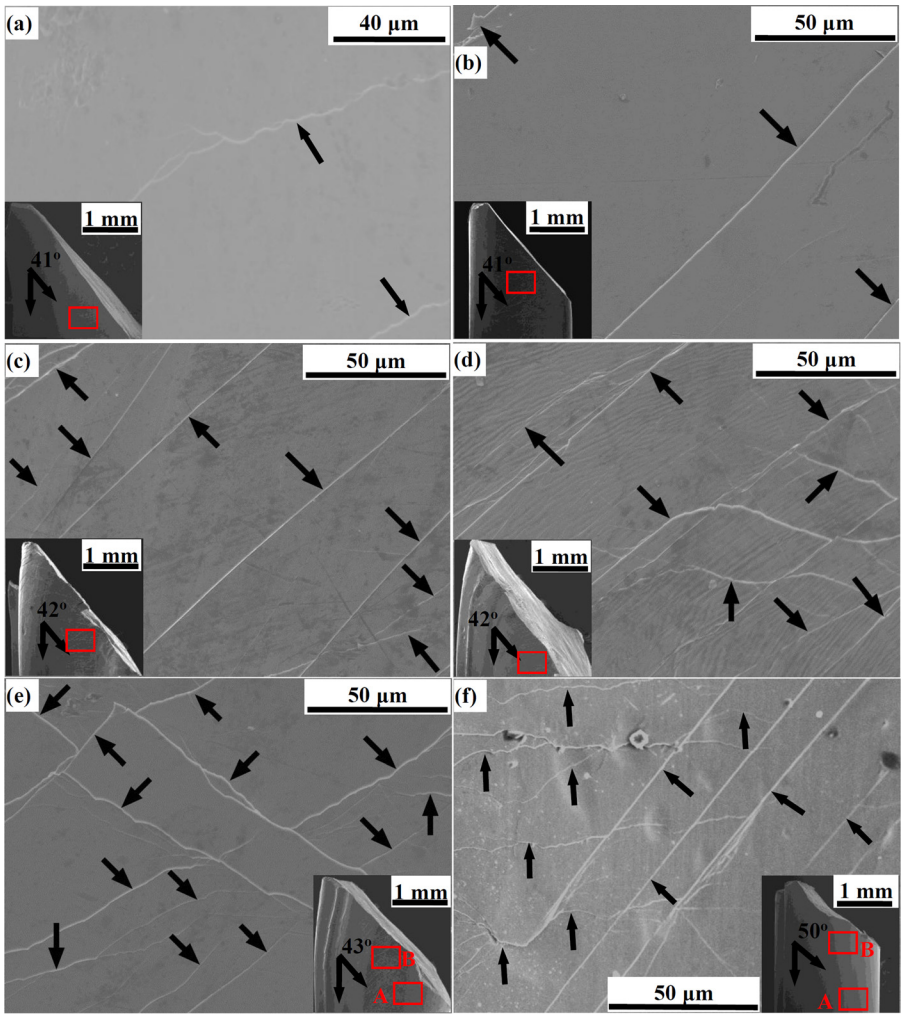

FIG. 5. Lateral surface morphologies of the fractured metallic glass at different temperatures, corresponding to the areas indicated by rectangles in the insets. The insets show the shear fracture angle. The arrows indicate shear bands, roughly reflecting the density of the shear bands. (a) 293 K, (b) 273 K, (c) 213 K, (d) 203 K, (e) 183 K, (f) 123 K (morphology reflects area A of the inset).

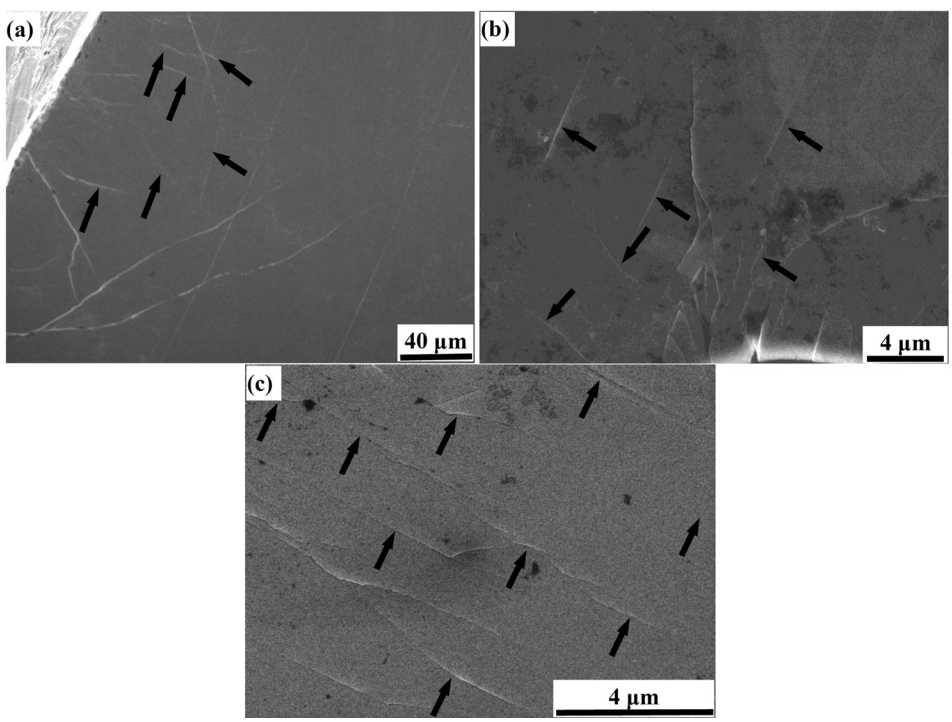

FIG. 6. Enlarged lateral surface of the fractured metallic glass at different temperatures. (a) 203 K: morphology near the fracture surface. (b) 183 K: morphology corresponding to the area indicated by B in the inset of Fig. 5(e). (c) 123 K: morphology corresponding to the area indicated by B in the inset of Fig. 5(f).

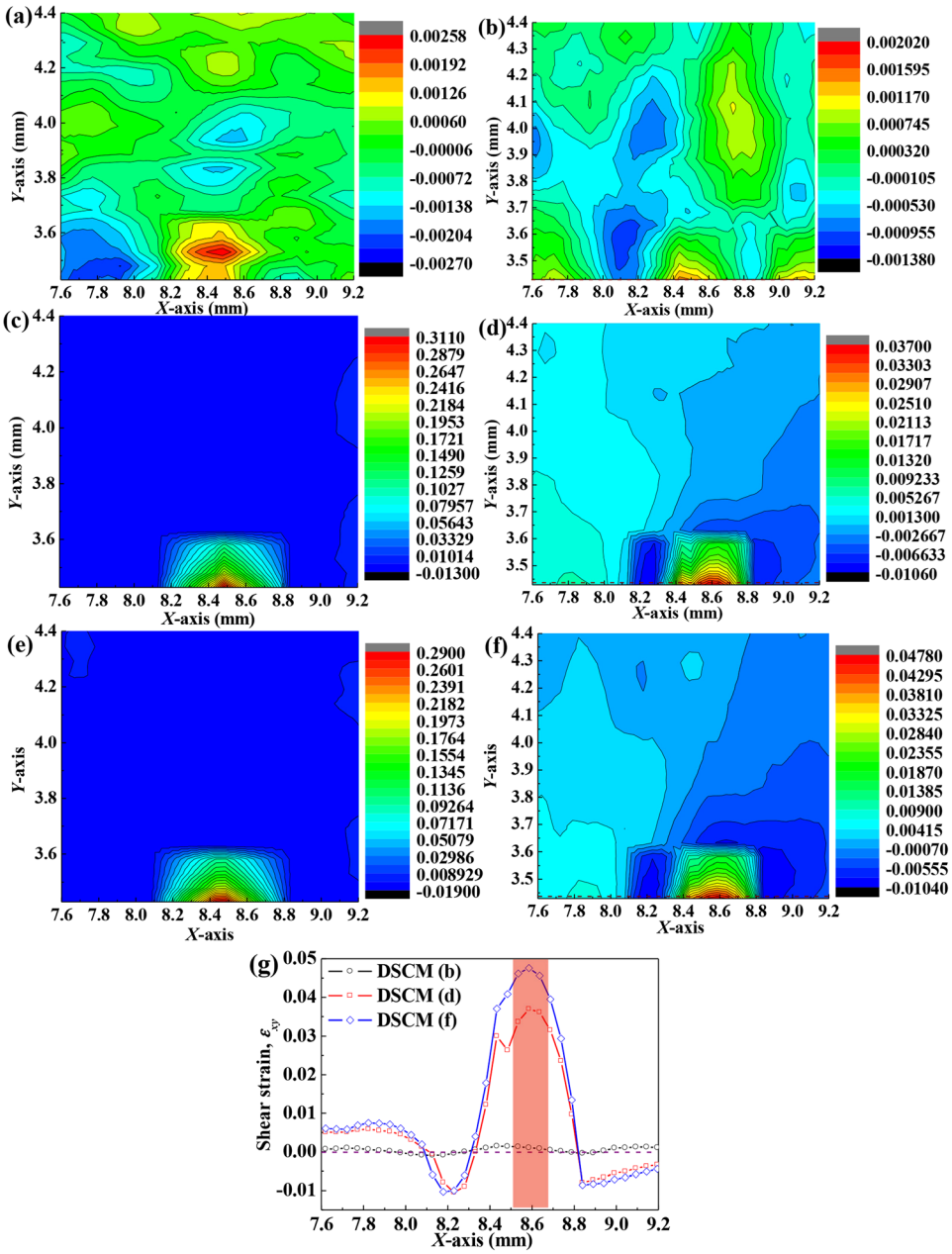

FIG. 7. DSCM observation of the elastic strain field of the $Zr_{41.25}Ti_{13.75}Ni_{10}Cu_{12.5}Be_{22.5}$ metallic glass beneath the loading point. The *X*-axis and *Y*-axis indicate the width of elastic strain field and loading direction, respectively. Dash lines in (b), (d), and (f) point to the direction perpendicular to the loading direction and the position close to the loading point. (a), (c), and (e) Contour maps of the linear strain (along the loading direction) field at loads of 10 N, 360 N, and 500 N, respectively. (b), (d), and (f) Contour maps of the shear strain field at a load of 10 N, 360 N, and 500 N, respectively. (g) Shear strain distribution along the *X*-axis under the indenter tip.

temperature, we can see that the elastic modulus does not increase linearly with decreasing temperature. A previous study by Varshni has deduced an equation to describe the evolution of the elastic constants with temperature, that can be expressed as,[25]

$$C_T = C_0 - \frac{S}{\exp[\theta/T] - 1}, \quad (1)$$

where C_T and C_0 are the elastic constants (which can be elastic modulus, shear modulus, or bulk modulus) at different temperatures and 0 K, respectively, θ is the effective Einstein temperature, and S is an adjustable parameter related to the strength of the anharmonic interactions.[26,27] Figure 8(a) clearly shows that Eq. (1) can well fit the elastic modulus experimentally measured in the temperature range from 123 K to room temperature. The fitting parameters are also listed in Fig. 8(a). Using these fitting parameters and the shear modulus experimentally measured at room temperature (Fig. 4), the shear modulus as a function of low temperatures is plotted in Fig. 8(b). The shear modulus at 0 K is calculated to be 35.4 GPa, as shown in Fig. 8(b). It is obvious that an increase of temperature from 123 K to 293 K results in a shear modulus decrease from 35.2 GPa to 32.5 GPa, a reduction of 8.4% in shear modulus.

After yielding, the elastic energy must activate atomic reorientation, and then form concordantly shifting regions.[28] These concordantly shifting regions act as primary deformation units to render plastic strain and are the so-called shear transition zones (STZs). The activation energy of one STZ, W, can be estimated by $W = (8/\pi^2)\gamma_C{}^2 G\Omega$, where G is the shear modulus, Ω is the effective STZ volume, and γ_c is a critical shear strain for metallic glasses, which was found to be a constant (0.036).[5,29] Accordingly, the activation energy is dominated by the shear modulus and the effective activation volume of STZ. The activation volume of an STZ increases

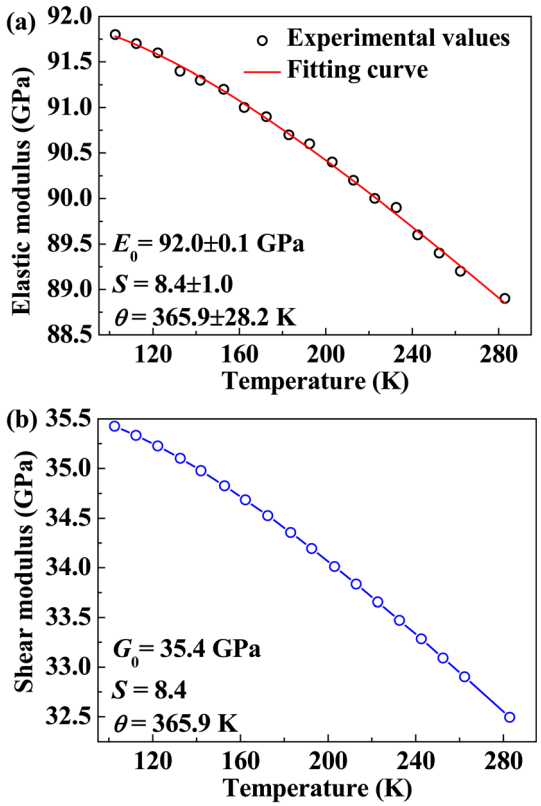

FIG. 8. Elastic modulus and shear modulus change with temperature ranging from 123 K to room temperature. (a) The experimental elastic modulus. (b) The shear modulus calculated by the Varshni equation.

with the decreasing temperature.[13] Thus, the activation energy of STZ increases with the temperature decrease from room temperature to 123 K. The concordantly shifting of the atoms in STZs required more activation energy at low temperatures compared with that at room temperature, which results in a higher yield strength at low temperature.

After yielding, the shear banding behaviour commences to dominate the deformation process. With the temperature decreasing, the density of the shear bands increases. The elastic shear strain field measurements by DSCM suggest that the size of the elastic shear strain field is as large as 600 μm (cf. Fig. 7) which is almost six times larger than the maximum interval space ($\sim$100 μm) of the shear bands. Thus, the interaction between the shear strain fields initiated from neighbouring shear bands must influence the shear banding behaviour in the spatial dimension.[30,31] With the temperature decreasing, the interval space of the shear bands decreases, suggesting that the interaction of the elastic shear strain fields initiated from different shear bands are enhanced.[31] This possibly generates a highly localized stress level, bringing out a localized yielding behaviour.[32] Numerous very weak shear bands at the shortened length scale observed by the SEM provide direct evidence that a very localized yielding behaviour is occurring (cf. Fig. 6). Since the shear banding behaviour is manifested as the serrated flow behaviour in the plastic regime, the decrease in the amplitude of the serration events must correspond to the shear avalanche size reduction. The stress-time curves show that the fluctuation of the serration event becomes indistinct with decreasing temperature and is totally covered by the background noise when the temperature is lower than 203 K, which is consistent with the shear band observation results shown in Figs. 5 and 6. In this case, we can image that the formation of shear bands in small length scale partitions the elastic energy in each serration event. This can bring out the plastic flow to avoid the occurrence of the large shear avalanche, and therefore improve the plastic deformation ability.

After fracture, the SEM images show that the fracture angle changes when the temperature decreases, suggesting that the critical shear stress and the critical shear strain are influenced by the shear fracture angle besides the yield strength of the metallic glass. The critical shear stress at different temperatures can be calculated by $\tau_{CT} = \sigma_{FT} \sin\theta_T \cos\theta_T$,[33,34] where σ_{FT} and θ_T are the fracture stress and the fracture angle at different temperatures, respectively. The fracture angle can be measured directly using the SEM results (Fig. 5), and the fracture stress is determined from Fig. 2 (Table I). The calculated critical shear stress values at different temperatures are also listed in Table I, which shows an increase with decreasing temperature. Thus, low temperature seems to freeze the shear flow behaviour.

V. CONCLUSIONS

Plastic serrated flow of the $Zr_{41.25}Ti_{13.75}Ni_{10}Cu_{12.5}Be_{22.5}$ metallic glass at different temperatures well below the glassy transition temperature is experimentally investigated. Low temperatures can increase the size and the activation energy required of STZs, which significantly improves the yield strength of the metallic glass. The shear band density increase at low temperatures indicates that interactions between the elastic strain fields of neighbouring shear bands are enhanced by the decreasing interval space of the shear bands. Experimentally observations and linearly elastic strain field analysis suggest that the shear bands tend to operate cooperatively due to their enhanced mutual long-range elastic field interactions which activate localized yielding to bring out the shear bands in small length scales. Subsequently, these shear avalanches at small scales can knife the elastic energy in each serration event, which is manifested in the observed smooth plastic flow of metallic glass at low temperatures.

ACKNOWLEDGMENTS

The work described in this paper was supported by a grant from the Research Grants Council of the Hong Kong Special Administrative Region, China (Project No. e.g. PolyU511211), grants from the NSF of China (Nos. 51171098, 51222102, and 11271339) and the NCET (10-0141) program, the Shanghai Pujiang Program (Nr. 11PJ1403900), the Innovation Program of Shanghai Municipal Education Commission (Nr. 12ZZ090), the Program for Professor of Special Appointment (Eastern Scholar) at Shanghai Institutions of Higher Learning, and the 085 project in Shanghai University.

[1]D. Klaumünzer, A. Lazarev, R. Maaß, F. H. Dalla Torre, A. Vinogradov, and J. F. Löffler, Phys. Rev. Lett. **107**, 185502 (2011).
[2]B. A. Sun, H. B. Yu, W. Jiao, H. Y. Bai, D. Q. Zhao, and W. H. Wang, Phys. Rev. Lett. **105**, 035501 (2010).

[3]C. A. Schuh and A. C. Lund, Nat. Mater. **2**, 449 (2003).
[4]F. Spaepen, Acta Metall. **25**, 407 (1977).
[5]J. Schroers and W. L. Johnson, Phys. Rev. Lett. **93**, 255506 (2004).
[6]D. Pan, A. Inoue, T. Sakurai, and M. W. Chen, PNAS **105**, 14769 (2008).
[7]M. L. Falk and J. S. Langer, MRS Bull. **25**, 40 (2000).
[8]S. G. Mayr, Phys. Rev. Lett. **97**, 195501 (2006).
[9]W. L. Johnson and K. Samwer, Phys. Rev. Lett. **95**, 195501 (2005).
[10]R. Sarmah, G. Ananthakrishna, B. A. Sun, and W. H. Wang, Acta Mater. **59**, 4482 (2011).
[11]G. Wang, I. Jackson, J. D. Fitz Gerald, J. Shen, and Z. H. Stachurski, J. Non-Cryst. Solids **354**, 1575 (2008).
[12]J. Lu, G. Ravichandran, and W. L. Johnson, Acta Mater. **51**, 3429 (2003).
[13]D. Pan, H. Guo, W. Zhang, A. Inoue, and M. W. Chen, Appl. Phys. Lett. **99**, 241907 (2011).
[14]F. Jiang, M. Q. Jiang, H. F. Wang, Y. L. Zhao, L. He, and J. Sun, Acta Mater. **59**, 2057 (2011).
[15]D. Klaumünzer, R. Maaß, F. H. Dalla Torre, and J. F. Löffler, Appl. Phys. Lett. **96**, 061901 (2010).
[16]K.-S. Yoon, M. Lee, E. Fleury, and J.-C. Lee, Acta Mater. **58**, 5295 (2010).
[17]J. W. Qiao, H. L. Jia, Y. Zhang, P. K. Liaw, and L. F. Li, Mater. Chem. Phys. **136**, 75 (2012).
[18]H. Q. Li, C. Fan, K. X. Tao, H. Choo, and P. K. Liaw, Adv. Mater. **18**, 752 (2006).
[19]X. H. Xu, S. P. Ma, M. F. Xia, F. J. Ke, and Y. L. Bai, Theor. Appl. Fract. Mech. **44**, 146 (2005).
[20]G. Wang, X. H. Xu, F. J. Ke, and W. H. Wang, J. Appl. Phys. **104**, 073530 (2008).
[21]G. Wang, J. Shen, Q. H. Qin, J. F. Sun, Z. H. Stachurski, and B. D. Zhou, J. Mater. Sci. **40**, 4561 (2005).
[22]W. L. Johnson, M. D. Demetriou, J. S. Harmon, M. L. Lind, and K. Samwer, MRS Bull. **32**, 644 (2007).
[23]Y. Suzuki, J. Haimovich, and T. Egami, Phys. Rev. B **35**, 2162 (1987).
[24]N. Mattern, J. Bednarčik, S. Pauly, G. Wang, J. Das, and J. Eckert, Acta Mater. **57**, 4133 (2009).
[25]Y. P. Varshni, Phys. Rev. B **2**, 3952 (1970).
[26]P. Yu, R. J. Wang, D. Q. Zhao, and H. Y. Bai, Appl. Phys. Lett. **90**, 251904 (2007).
[27]W. H. Wang, Prog. Mater. Sci. **57**, 487 (2012).
[28]G. Wang, N. Mattern, J. Bednarčík, R. Li, B. Zhang, and J. Eckert, Acta Mater. **60**, 3074 (2012).
[29]M. D. Demetriou, J. S. Harmon, M. Tao, G. Duan, K. Samwer, and W. L. Johnson, Phys. Rev. Lett. **97**, 065502 (2006).
[30]Y. Estrin and L. P. Kubin, *Continuum Models for Materials with Microsctructures* (Wiley, New York, 1995).
[31]G. E. Dieter, *Mechanical Metallurgy*, 3rd ed. (McGraw Hill Companies, Inc., 2006).
[32]Y. Tanaka, Y. Kawauchi, T. Kurokawa, H. Furukawa, T. Okajima, and J. P. Gong, Macromol. Rapid Commun. **29**, 1514 (2008).
[33]P. E. Donovan, Acta Mater. **37**, 445 (1989).
[34]Z. F. Zhang and J. Eckert, Phys. Rev. Lett. **94**, 094301 (2005).